# Midlatitude Excitation of Tropical Variability in the Pacific: The Role of Thermodynamic Coupling and Seasonality*

DANIEL J. VIMONT

*Department of Atmospheric and Oceanic Sciences, and Center for Climatic Research, University of Wisconsin—Madison, Madison, Wisconsin*

MICHAEL ALEXANDER

*NOAA/Earth Systems Research Laboratory, Boulder, Colorado*

ABIGAIL FONTAINE

*Department of Atmospheric and Oceanic Sciences, and Center for Climatic Research, University of Wisconsin—Madison, Madison, Wisconsin*

(Manuscript received 6 September 2007, in final form 20 May 2008)

ABSTRACT

A set of ensemble model experiments using the National Center for Atmospheric Research Community Atmospheric Model version 3.0 (CAM3) is run to investigate the tropical Pacific response to midlatitude atmospheric variability associated with the atmospheric North Pacific Oscillation (NPO). Heat flux anomalies associated with the NPO are used to force a set of model simulations during boreal winter (when the NPO is most energetic), after which the forcing is switched off and the coupled model evolves on its own. Sea surface temperature (SST) and wind anomalies continue to amplify in the tropical Pacific after the imposed forcing has been shut off, indicating that coupled ocean–atmosphere interactions in the tropical Pacific alter the spatial and temporal structure of variability associated with midlatitude forcing. The tropical circulation evolves through feedbacks between the surface wind, evaporation, and SST (the WES feedback), as well as through changes in the shortwave radiative heat flux (caused by changes in convection).

Sensitivity experiments are run to investigate how thermodynamic coupling and seasonality affect the tropical response to NPO-related forcing. Seasonality is found to affect the WES feedback through (i) altering the sensitivity of surface evaporation to changes in the low-level wind field and (ii) altering the structure and strength of the lower-level wind response to SST anomalies. Thermodynamic coupling causes an equatorward and westward development of SST anomalies and an associated equatorward shift in the lower-level zonal wind anomalies.

## 1. Introduction

Interannual and decadal variations in the tropical Pacific associated with the El Niño–Southern Oscillation (ENSO) and ENSO-like decadal variability (Zhang et al. 1997) are closely tied to midlatitude atmospheric variability both through tropical influences on the midlatitudes via the ''atmospheric bridge'' (Nitta and Yamada 1989; Alexander 1992a,b; Lau 1997; Trenberth et al. 1998; Alexander et al. 2002) and through midlatitude atmospheric influence on the tropical circulation (Barnett et al. 1999; Pierce et al. 2000; Vimont et al. 2001, 2003a,b; Vimont 2005; Alexander et al. 2008). In this study we investigate the dynamics of the latter connection—the midlatitude influence on tropical variability. In particular, we investigate how a dominant pattern of atmospheric variability in North Pacific, the North Pacific Oscillation (NPO; Walker and Bliss 1932;

* Center for Climatic Research Contribution Number 952.

*Corresponding author address:* Daniel J. Vimont, 1225 W. Dayton St., Madison, WI 53706.
E-mail: dvimont@wisc.edu

DOI: 10.1175/2008JCLI2220.1

Rogers 1981; Linkin and Nigam 2008), excites coupled dynamical feedbacks in the subtropical and tropical Pacific.

The role of midlatitude atmospheric variability in exciting tropical coupled variations has been demonstrated in both the Pacific and Atlantic basins. In the Atlantic, trade wind variations associated with the North Atlantic Oscillation (NAO) alter subtropical SST through changes in surface latent heat flux (Xie and Tanimoto 1998; Czaja et al. 2002). The resulting SST anomalies excite a tropical response that includes a shift in the intertropical convergence zone (ITCZ) and cross-equatorial boundary layer flow toward the warmer hemisphere (Hastenrath and Heller 1977). An important component of the lower-level flow includes a veering of the winds to the right (left) in the Northern (Southern) Hemisphere, in accord with the Coriolis force, that results in a relaxation (intensification) of the lower-level trades in the warmer (colder) hemisphere. These trade wind fluctuations change evaporation leading to a positive feedback on the original SST anomaly. This positive feedback between wind, evaporation, and SST (the WES feedback; Xie and Philander 1994; Chang et al. 1997) has been shown to play an important role in tropical ''meridional mode'' variations in the Atlantic in observations (Czaja et al. 2002, Chiang and Vimont 2004; Hu and Huang 2006), in theoretical analyses (Xie 1997, 1999), and more complete coupled models (Carton et al. 1996; Chang et al. 1997, 2000).

Midlatitude variability associated with the NPO in the Pacific appears to excite a similar sequence of variations in the subtropical and tropical Pacific (Vimont et al. 2001, 2003a,b; Chiang and Vimont 2004; Chang et al. 2007). The NPO-forced subtropical SST anomalies excite an atmospheric circulation that includes zonal wind anomalies that extend into the deep tropics; these wind anomalies are responsible for exciting or altering subsequent ENSO events (Barnett et al. 1999; Pierce et al. 2000; Anderson 2003; Vimont et al. 2003a,b). Anderson and Maloney (2006) show that sea level pressure (SLP) precursors to ENSO variability are present in an earlier, fully coupled version of the model used in the present study.

The excitation of tropical variability by midlatitude processes is regulated by the seasonality of midlatitude variability (the forcing process) and seasonality associated with the coupled response. The seasonality of tropical Atlantic variability is strongly influenced by the boreal winter NAO variations, as well as the seasonal response to ENSO (Chang et al. 2000; Czaja 2004). In the Pacific, the seasonality of midlatitude atmospheric variability can affect ENSO's phase locking to the seasonal cycle (Chang et al. 2007). This suggests an important role for midlatitude seasonality in altering tropical Pacific variability. The WES feedback itself involves three different processes that are sensitive to the mean state and seasonal cycle: (i) wind variations generate changes in surface evaporation (e.g., evaporation changes depend on the mean wind speed), (ii) surface evaporation alters the underlying SST (e.g., the amount of SST change depends on the mixed layer depth, which varies seasonally), and (iii) the resulting SST anomalies generate atmospheric circulation anomalies that, if the WES feedback is to be positive, should resemble the original wind variations (the atmospheric response depends on the mean ITCZ location; e.g., Okajima et al. 2003). In the present study, we focus on how seasonality affects the first and third processes (section 5, below).

Two approaches could be used to investigate the midlatitude influence on tropical variability: analysis of a long coupled simulation (e.g., Vimont et al. 2001, 2003a), or specific experiments that isolate the response to a specific forcing. In this study we choose the latter approach, and design a set of coupled and uncoupled general circulation model experiments with prescribed surface flux forcing associated with the NPO to investigate its potential influence on the tropical circulation. The model and experimental design are explained in section 2, and the imposed NPO-related forcing is described in section 3. The model response to imposed NPO heat flux forcing is described in section 4, followed by a discussion of seasonality and the WES feedback in the Pacific in section 5. Finally, a discussion of results is presented in section 6.

## 2. Model description and experimental design

### *a. Model description*

Model experiments are conducted using the National Center for Atmospheric Research (NCAR) Community Atmospheric Model, version 3.0 (CAM3; Collins et al. 2004, 2006a,b). The model is run at T42 resolution (approximately 2.8° resolution in physical space), with 26 vertical levels and a 20-min time step. The surface sensible and latent heat flux is calculated using a standard bulk formula (see section 4c) that includes a stability-dependent transfer coefficient. CAM3 can be run in an uncoupled setting by imposing the observed climatological seasonal cycle as a lower boundary condition. We obtained 200 yr of data from a long uncoupled control simulation (CAM3 control; Table 1) that had been run at NCAR by A. Phillips. A set of sensitivity experiments is also run in which the SST climatology is altered by imposing SST anomalies in the

TABLE 1. Summary of model simulations used throughout the study.

| Name | Model | Forcing/initial value | Notes |
|---|---|---|---|
| CAM3 control (200 yr) | Uncoupled CAM3 (no SST evolution) | None | Used to calculate imposed NPO forcing and to generate Q flux. (Fig. 1b) |
| CAM3 + SOM control | CAM3 + SOM | None | 20-yr continuous simulation. Last 10 yr used for analysis (Figs. 4, 5, and 6) and initial conditions |
| NPO-WARM<br>NPO-COLD | CAM3 + SOM | 2 × NPO heat flux imposed from November to March (Fig. 1b) | Two ensemble simulations (10 members) initialized in November, and run for 18 months each (Figs. 2, 3, 4) |
| CAM3 SST-forced | Uncoupled CAM3 (no SST evolution) | Idealized SST (Fig. 8a) | Two 10-yr simulations with opposite polarity of SST forcing (Fig. 7) |
| IVP: (April, July, October, January initialized) | CAM3 + SOM | Idealized heat content anomaly (corresponds identically to the SST anomaly in Fig. 8a) | Ensemble simulations (both polarities of the initial heat content anomaly; 10 members each) initialized in July (JulIvp) and April (AprIvp) and run for 6 months |

eastern subtropical Pacific (section 5). The SST climatology is described in Collins et al. (2004) and is the average annual cycle from the Reynolds et al. (2002) dataset over the time period 1981–2001. Additional details of the model, including analysis of the model mean state and variability, can be found in a special issue of the *Journal of Climate* (2006, Vol. 19, No. 11) devoted to the Community Climate System Model (CCSM).

For most experiments in the present study, CAM3 is coupled to a uniform depth, motionless, 50-m slab ocean model (SOM), which allows the coupled system to generate its own SST variability. The SOM represents a uniform (well mixed) oceanic mixed layer that determines SST through integrating the net surface heat flux. To account for oceanic heat transports and model biases a flux correction (Q flux) is applied to the SOM (appendix A; Collins et al. 2004). The Q flux applied at each time step is a linear interpolation of midmonthly values from the current and closest surrounding months (e.g., the Q flux for 1 November would be a weighted average of the October and November Q flux). A control simulation of the CAM3 + SOM is run for 20 yr, of which the last 10 yr are used to generate initial conditions for the ensemble experiments, and for analysis.

### b. Experimental design

To separate the effect of midlatitude forcing from tropical coupled processes we run ensembles of model simulations. Three experiments are conducted: (i) a boundary-forced experiment in which the NPO-related surface heat flux is imposed as a forcing to the CAM3 + SOM, (ii) a boundary-forced experiment in which an idealized SST anomaly is used to force the uncoupled CAM3 model, and (iii) an experiment in which the same idealized SST (heat content) anomaly is used to initialize a set of CAM3 + SOM simulations. For reference all experiments in the present study are summarized in Table 1 and described further below.

The NPO-forced experiments are conducted as follows. During boreal winter [November–March (NDJFM)] when the NPO is most energetic, the oceanic mixed layer is driven by an external forcing by adding the NPO-related heat flux anomaly to the Q flux (Fig. 1b; described below). The imposed forcing is turned off in April and the model variability evolves via its own coupled dynamics and feedbacks. Because of the linear interpolation from the monthly Q-flux field to the model's 20-min time step, the imposed forcing gradually increases to full strength by mid-November, and gradually decreases from full strength in mid-March to zero amplitude by mid-April. The model is then run without any imposed forcing through the following April (18 months total). We note that the experimental formulation may include redundancy between imposed NPO-related heat flux and internally generated NPO variability in any individual model simulation. To minimize the influence of internally generated variability we run an ensemble of model simulations so that averaging across the individual members, each of which should contain internal variability that is incoherent with other ensemble members, will emphasize the NPO-forced model response. Although this linear assumption is an oversimplification, the coherent model response throughout the study is taken as evidence that the experimental design is appropriate for addressing the NPO's influence on tropical climate variability.

In section 5 we investigate the role of seasonality and the WES feedback by running ensemble simulations using an idealized SST anomaly as a forcing for the uncoupled CAM3 (an uncoupled, 10-yr simulation with constant forcing; "CAM3 SST-forced" in Table 1), or as

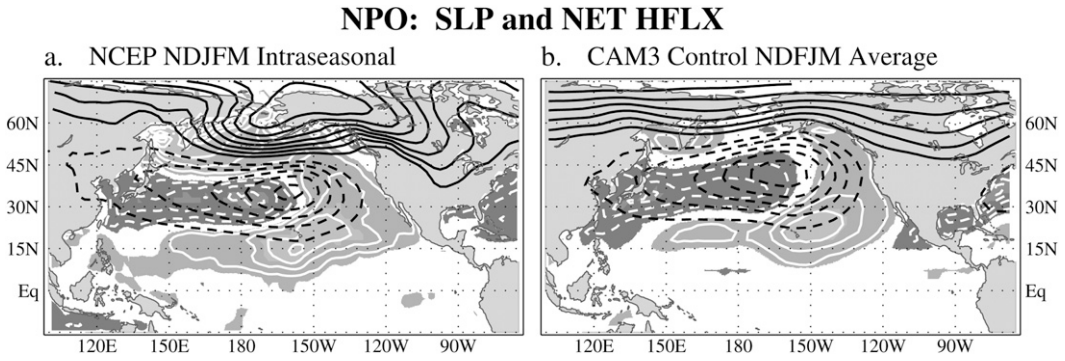


FIG. 1. Wintertime SLP [black contours; 0.5 mb (std dev)$^{-1}$] and net surface heat flux [white contours and shading; 5 W m$^{-2}$ (std dev)$^{-1}$] anomalies associated with the NPO. Results are presented for (a) intraseasonal time scales from the observed NCEP reanalysis record, and (b) the CAM3 control simulation. Solid contours denote positive anomalies, dashed contours denote negative anomalies, and the zero contour has been omitted. See text for a description of how the two maps are derived. The imposed heat flux for the forced ensemble simulations is twice the heat flux map in (b).

an initial heat content anomaly for the CAM3 + SOM [an ''initial value problem'' (IVP) in Table 1]. The idealized SST or heat content anomalies have a Gaussian shape in the meridional direction with an *e*-folding width of 7.5° and a cosine shape in the zonal direction with a width of 60° centered at 22.5°N, 150°W, with a maximum amplitude corresponding to 1°C. This shape and amplitude is motivated by the response to the NPO-forced CAM3 + SOM experiments (section 3). For the IVP experiment, we run four experiments initialized with the idealized heat content anomalies in April, July, October, and January (Table 1).

Two ensembles of model simulations are run for each experiment, corresponding to positive or negative polarity of the forcing or initial condition. To reduce sampling error, each ensemble contains 10 individual model simulations initiated from different initial conditions (taken from each 1 November during the last 10 years of the CAM3 + SOM control simulation). The heat flux anomalies in the NPO-forced experiments (defined below) are those that would correspond to a two standard deviation anomaly of the NPO (thus, the heat flux anomalies in Fig. 1b are multiplied by 2). By convention, experiments with positive (negative) heat flux forcing or positive (negative) SST anomalies in the eastern subtropical Pacific are labeled WARM (COLD) experiments, and downward heat flux is positive. Results are presented as one-half the difference between the WARM and COLD ensemble averages. Statistical significance is inferred using a standard *t* test on the difference in means of the WARM or COLD ensemble. Unless otherwise stated, we restrict discussion in the present manuscript to ensemble mean differences that are statistically significant at the 95% confidence level, assuming a 2-tailed Student's *t* test.

## 3. Uncoupled NPO-related heat flux forcing

The imposed NPO-related forcing (NPO-WARM and NPO-COLD experiments; Table 1) is designed to represent heat flux anomalies associated with the NPO in the absence of coupling. In a coupled system the net heat flux contains contributions from atmospheric forcing and the response to that forcing. We use two different methods to estimate the atmospheric contribution to the NPO-related heat flux forcing, the results of which are compared in Fig. 1. The first method uses existing observations from the National Centers for Environmental Prediction (NCEP)–NCAR reanalysis project (Kalnay et al. 1996), and the differing time scales of oceanic and atmospheric variations. We apply an intraseasonal filter to distinguish between the atmospheric (higher frequency) and oceanic (lower frequency due to the thermal inertia of the oceanic mixed layer) contributions to the net surface heat flux. In the second method, the atmospheric contribution to the heat flux is defined in the long uncoupled CAM3 control simulation (Table 1), which includes no oceanic contribution as the SST is fixed to climatology.

The NPO is defined from the NCEP reanalysis by applying empirical orthogonal function/principal component (EOF/PC) analysis to the intraseasonal boreal winter (NDJFM) SLP anomalies over the North Pacific (20°–90°N, 110°E–70°W) and over the time period 1948–2002. The intraseasonal data is generated by (i) removing the annual cycle from the SLP data by subtracting the mean for each calendar month, then (ii) subtracting each winter's mean from the corresponding monthly data. Although this does not eliminate all coupled variability, it significantly reduces the interannual variability associated with ENSO or with local coupled

ocean–atmosphere interactions. The second EOF (19% variance explained) represents variability of the NPO and is well separated from the first EOF (the Aleutian low, 26% variance explained) and the higher-order EOFs (11% variance explained or less). For reference, the NPO is related to the west Pacific teleconnection pattern at upper levels and involves a meridional shift in the climatological jet location (Hsu and Wallace 1985; Linkin and Nigam 2008), and the Aleutian low is related to the Pacific–North America teleconnection pattern (Wallace and Gutzler 1981; Ambaum et al. 2001; Quadrelli and Wallace 2004). Finally, the intraseasonal net surface heat flux is regressed onto the second PC time series to obtain the net surface heat flux variability associated with one standard deviation of the intraseasonal NPO. Regression maps of intraseasonal SLP and heat flux anomalies onto the observed standardized second PC time series are plotted in Fig. 1a.

The second method defines the NPO in the long (200 yr) uncoupled CAM3 control simulation. EOF analysis is applied to the winter (NDJFM) averaged SLP anomalies (over the same region), and the net heat flux is regressed onto the second PC time series (26% variance explained; the leading EOF represents the Aleutian low and explains 35% of the variance; higher-order modes explain 11% or less). Regression maps of SLP and heat flux onto the model's standardized second PC time series are plotted in Fig. 1b. The amplitudes of both maps may be directly compared as they represent the amplitude of anomalies per standard deviation of the associated NPO time series.

Both the modeled and observed NPO share similar structures in their SLP and heat flux maps, and bear a strong resemblance to analysis of the second EOF of maritime SLP and its associated heat flux by Cayan (1992) using a different dataset. An important feature of the SLP maps is a low pressure anomaly centered around 35°–40°N. The surface wind anomalies along the southern flank of this SLP anomaly reduce the climatological trade wind strength and consequently reduce the upward turbulent heat flux from the ocean surface (this turbulent heat flux is dominated by the latent heat flux; see also Cayan 1992). In both the model and observations, a zonally elongated band of positive (downward) heat flux anomalies extends across the subtropical and tropical Pacific, from around 150°E to the eastern edge of the basin. These heat flux anomalies extend far enough equatorward to have an important effect on the tropical climate. In the midlatitudes, a band of negative (upward) heat flux anomalies extends from the west into the central North Pacific.

Despite the similarities between the observed and modeled variability, there are subtle differences in the NPO structure. In particular, the modeled NPO structure has a more hemispheric signature representative of the northern annular mode (NAM); the modeled annular mode is known to be overly coherent between the Pacific and Atlantic sectors. We note that the observed NPO does not resemble the observed NAM over the Pacific sector and indeed is nearly orthogonal to the observed NAM (NAM variations in the Pacific sector more closely resemble variations in the Aleutian low, which are orthogonal to the NPO by construction). Differences in the net surface heat flux also exist that may affect details of the NPO's impact on tropical Pacific climate variability. Most notably, the anomalously low SLP in the model, and the corresponding subtropical heat flux anomalies, are centered about 5° north of the corresponding anomalies in the observational record. Differences may result from model error or differences in analysis techniques. We ran the NPO-WARM and NPO-COLD experiments with both heat flux anomalies, and found that results did not substantially differ. For consistency, results from the CAM3-generated heat flux anomaly pattern in Fig. 1b are shown in the present study.

## 4. Model response to NPO-related heat flux

### *a. Description of the model response*

The modeled response to the imposed net surface heat flux anomaly in Fig. 1b is shown for various seasons in Fig. 2. Model lower-level winds (defined as the mass-weighted average below 850 mb) are only shown where statistically significant at the 95% level based on a multivariate *t* test. During late boreal winter [January–March (JFM; year 1); Fig. 2a], the SST anomalies bear a strong resemblance to the imposed heat flux forcing during the winter, suggesting that the ensemble size is sufficient to eliminate much of the random model variability. Lower-level winds are weak at this time. Not surprisingly, the largest SST anomalies appear in eastern subtropics (around 20°N, 150°W), in the same location as the maximum downward heat flux anomalies (cf. Fig. 1). These subtropical SST anomalies develop through boreal winter and maximize in boreal spring, consistent with the phasing implied by integration of the imposed forcing (Hasselmann 1976), then decay through the remainder of the model simulation.

By boreal spring [April–June (AMJ); Fig. 2b], positive SST anomalies have spread into the northwestern tropical Pacific region (NWTP; 15°N–0°, 120°E–180°; for reference, this region is boxed in the first panel of each of the figures) despite weak *negative* (upward) heat flux anomalies imposed in that region from November

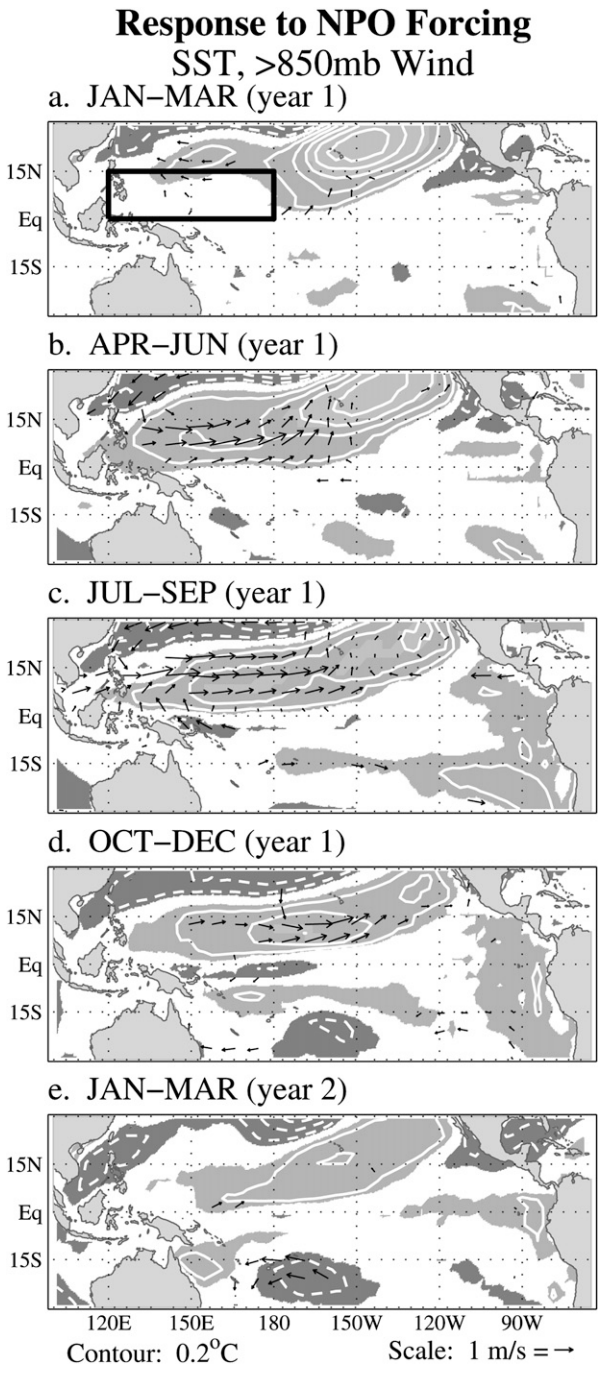


FIG. 2. NPO-WARM minus NPO-COLD simulation. Evolution of the model SST (shading and contours; 0.2°C) and lower-level wind (vectors; scale at the bottom of the last panel) response to the imposed surface heat flux. For SST, solid contours and light shading denote positive anomalies, dashed contours and dark shading denote negative anomalies, and the zero contour has been omitted. Anomalies are defied as one-half the difference in ensemble means between the WARM and COLD simulations (see text for description of model simulations). Lower-level winds are shown only where the difference in the ensemble mean wind vector is statistically significant at the 95% level based on a multivariate *t* test.

through March (though subtle, these are indicated by dark shading in Fig. 1b). This indicates that coupled feedbacks associated with the model response are acting to increase SST in that region during the imposed forcing period. The lower-level wind field shows a cyclonic circulation centered around 20°N and 165°E, including a zonal band of westerly anomalies in the NWTP. By boreal summer [July–September (JAS); Fig. 2c] SST anomalies in the NWTP have slightly amplified despite the removal of the imposed heat flux anomalies during the previous season. This amplification occurs in the region of relaxed lower-level trade winds, highlighting the role of coupled feedbacks in the evolution of tropical SST anomalies in the tropical Pacific.

Tropical SSTs continue to decay, though slowly, through boreal fall and into winter, as demonstrated in Figs. 2d,e. Of interest is the persistence and slight increase of SST anomalies around 10°N between the date line and 150°W through boreal fall [October–December (OND); Fig. 2d], and the development of two bands of negative SST anomalies near the date line and the equator in fall and near 20°S and 165°W during fall and the following winter. The positive SST anomalies are collocated with westerly wind anomalies, and the two negative SST anomalies are collocated with increased easterly winds. Again, this suggests an important role for coupled feedbacks. During the winter [JFM (year 2); Fig. 2e], SST and atmospheric circulation anomalies in the northern tropics continue to decay.

### *b. Heat budget in the NWTP*

To better understand the physical processes leading to the development of the NWTP SST anomalies, the heat budget for this region is plotted in Fig. 3. Note that in the SOM, the only process that can affect the anomalous SST is the net surface heat flux, comprising the net shortwave and longwave radiation, the turbulent sensible and latent heat fluxes, and any imposed forcing. Of these terms, it is found that only the latent and shortwave heat fluxes contribute appreciably to the heat budget.

Figure 3 shows that SST anomalies in the NWTP involve a period of amplification (February–June) and two periods of decay (June–September, and November onward) punctuated by a period of sustained SST (September–November). The amplification of SST anomalies during the February–June period occurs because of positive contributions from the latent and shortwave fluxes. During the latter half of this amplification (March–June), lower-level wind anomalies are opposed to the mean winds (Fig. 3, bottom; note that for plotting purposes, anomalous winds are scaled 4 times larger than mean winds in Fig. 3), implying a relaxation of the

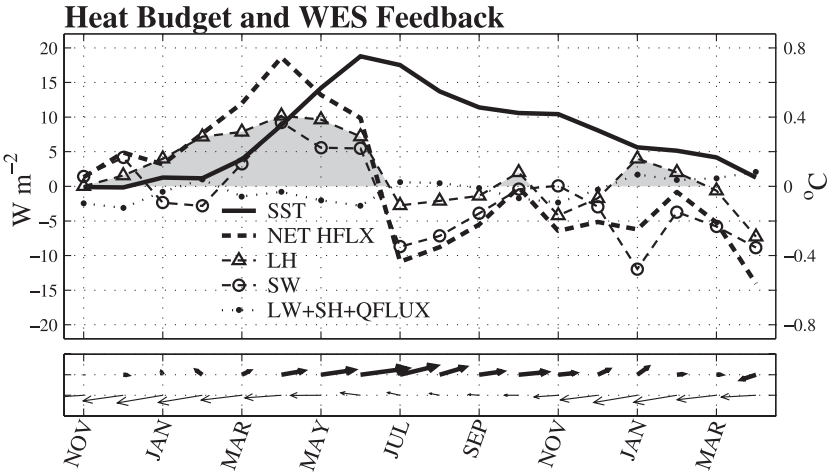


FIG. 3. NPO-WARM minus NPO-COLD simulation. Heat budget averaged over the NWTP region (15°N–0°, 120°E–180°; this region is boxed in Fig. 2a). Shown are the SST (thick solid line); net surface heat flux (thick dashed line); latent heat flux (dashed line with △); downward shortwave radiation (dashed line with ○); and the sum of the net surface longwave radiation, sensible heat flux, and imposed Q-flux (dotted line with •). Shading is used to emphasize the positive WES feedback over the region. Also shown are the anomalous (thick vectors) and mean (thin vectors) averaged lower-level wind anomalies (vector origins are collocated with the month that they represent). Note that for visualization, vector *anomalies* are scaled by 4 times the scaling for the *mean* winds. All anomalies are computed as one-half the difference of the WARM and COLD ensemble averages. By convention, downward heat flux anomalies are positive.

climatological trade wind strength and a reduction in the upward latent heat flux (a positive latent heat flux anomaly). This relationship demonstrates a positive WES feedback during this period of development. Shortwave heat fluxes also contribute to the boreal spring warming.

The cooling periods (June–September, and November onward) are caused mainly by negative shortwave heat flux anomalies (reduced downward shortwave radiation), with a small contribution from negative latent heat flux anomalies during boreal summer. It is noteworthy that the boreal summer (July–September) latent heat flux anomaly decreases considerably from the previous season, despite *stronger* lower-level wind anomalies in the NWTP region. This suggests that WES does not exert as strong a positive feedback over the NWTP region during boreal summer. During boreal fall (September–November), both latent and shortwave heat flux anomalies are near zero, despite warmer SST over the NWTP region. Again, the near-zero latent heat flux anomalies occur during a period of relaxed trade winds (i.e., westerly wind anomalies). The varying strength of the latent heat flux in Fig. 3, and its nonuniform relationship with the mean winds, suggests that the seasonal cycle plays an important role in altering the strength of the WES feedback in the tropical Pacific (section 5).

### c. *Surface heat flux components and the WES feedback*

The importance of coupled feedbacks in the evolution of SST anomalies in Fig. 3 motivates further analysis of the physical processes that contribute to the net surface heat flux. The net surface heat flux anomalies during boreal spring (AMJ) and summer (JAS) are contoured in Figs. 4a and 4b, respectively. For reference, underlying SST anomalies are shaded. In both of these seasons, the net surface heat flux tends to damp underlying SST anomalies over most of the subtropics. One exception is the NWTP region during boreal spring, where large downward heat flux anomalies are collocated with warm SSTs. During summer, heat flux anomalies in the NWTP generally act to damp underlying SSTs, though there is a region of downward heat flux over warm SST near the date line.

The shortwave and latent heat flux contributions to the net surface heat flux are contoured in the second and third rows of Fig. 4, respectively. Precipitation anomalies are shaded under the shortwave contours in Figs. 4c,d. In general, the shortwave heat flux follows changes in cloud amount, which can also be inferred from precipitation. During spring, the western tropical Pacific is characterized by a northward ITCZ shift, which

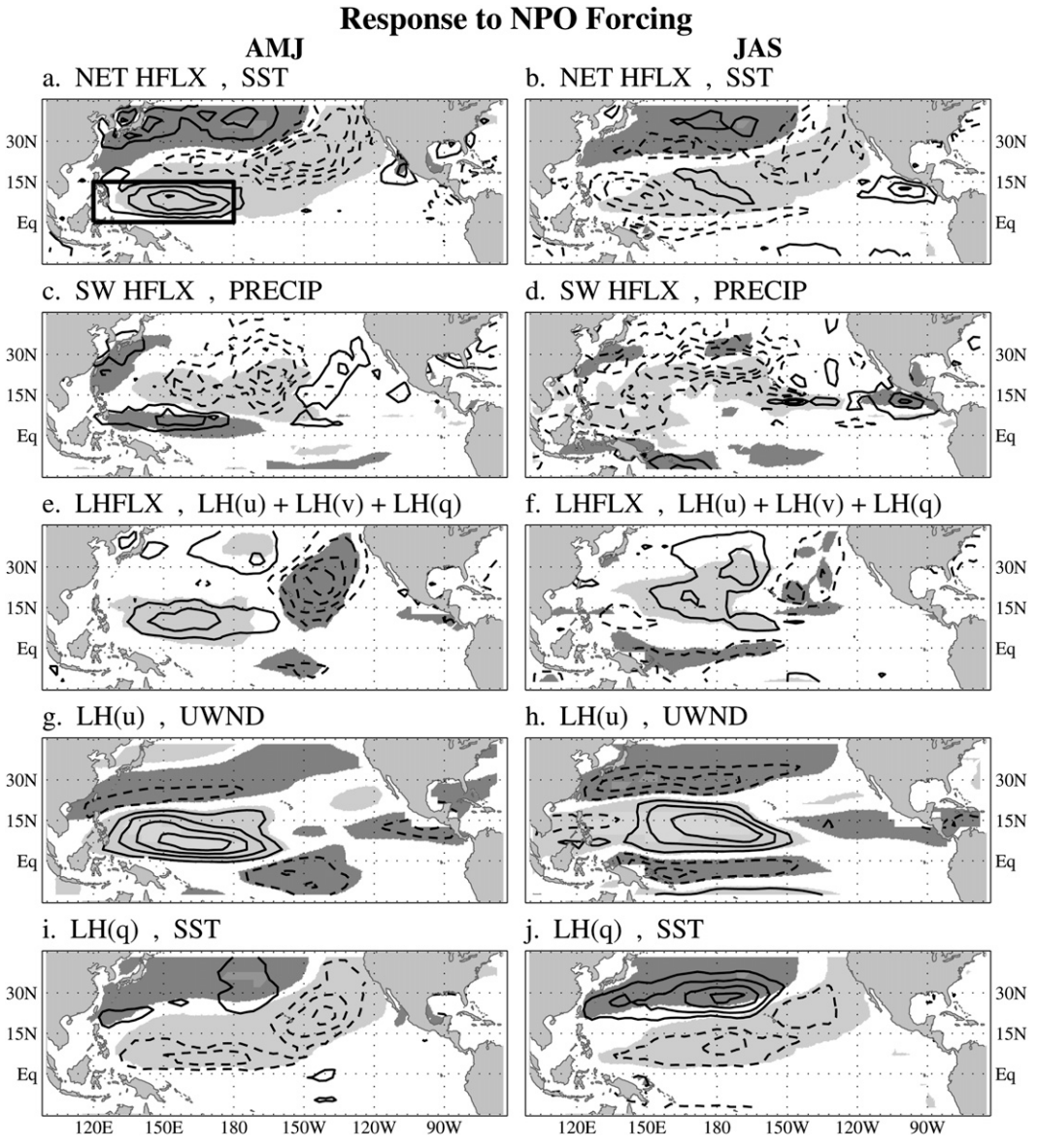


FIG. 4. NPO-WARM minus NPO-COLD simulation. Heat flux components from the NPO-forced CAM3 + SOM simulations during boreal spring (AMJ, left column) and summer (JAS, right column). Shown are (a), (b) net surface heat flux (contour 4 W $m^{-2}$) and SST (shaded where amplitude exceeds 0.2°C); (c), (d) downward shortwave radiation (contour 4 W $m^{-2}$) and precipitation (shaded where amplitude exceeds 0.4 mm $day^{-1}$); (e), (f) model latent heat flux (contour 4 W $m^{-2}$) and sum of bulk latent heat flux estimates from zonal wind, meridional wind, and humidity anomalies (shaded where amplitude exceeds 4 W $m^{-2}$); (g), (h) bulk latent heat flux estimates from zonal wind anomalies (contour 4 W $m^{-2}$) and actual zonal wind anomalies (shaded where amplitude exceeds 0.2 m $s^{-1}$); (i), (j) bulk latent heat flux estimate from humidity anomalies (contour 4 W $m^{-2}$) and SST anomalies (shaded where amplitude exceeds 0.2°C). In all panels positive values are denoted by solid contours (light shading), negative values are denoted by dashed lines (dark shading), and the zero contour has been omitted. By convention, downward heat flux anomalies are positive.

corresponds to a cloudiness reduction and redistribution over the NWTP region (downward shortwave anomalies accompanying reduced precipitation). In summer, precipitation anomalies are more disorganized (the mean ITCZ is also less confined in the western Pacific during summer) though there is a general increase in precipitation and decrease in downward shortwave radiation over the entire western subtropical Pacific. The model latent heat flux is contoured in Figs. 4e,f. During spring, the latent heat flux is characterized

by a large negative anomaly over the eastern subtropical Pacific (where the spring SST is at a maximum) and a positive anomaly over the NWTP region, where westerly wind anomalies are largest (Figs. 4g and 2b). We note that the positive (downward) net surface heat flux anomalies over the NWTP region involve equal contributions from the latent and shortwave heat fluxes.

Latent heat flux anomalies will result from changes in the surface wind speed and from changes in the vertical humidity gradient. We infer contributions from both processes by examining the contribution of zonal wind, or of the specific humidity gradient, to the total latent heat flux as follows. The bulk formula for calculating latent heat flux (LH) may be written

$$\mathrm{LH} = L_v C_e \rho_a [q_{\mathrm{sat}}(T_s) - \mathrm{RH} \cdot q_{\mathrm{sat}}(T_{\mathrm{ref}})]\bar{w}, \qquad (1)$$

where $L_v$ is the latent heat of vaporization ($2.5 \times 10^6$ J kg$^{-1}$), $C_e$ is an aerodynamic transfer coefficient (a function of stability and wind speed in the model; we use a constant value of $10^{-3}$), $\rho_a$ is the density of air (1.2 kg m$^{-3}$), $q_{\mathrm{sat}}(T)$ is the saturated specific humidity at temperature $T$, RH is the relative humidity at the lowest model level (about 65 m above the surface; relative humidity varies by only a few percent over the bottom 250 m), $T_s$ is the surface temperature, $T_{\mathrm{ref}}$ is the atmospheric temperature at a reference height of 2 m, and $\bar{w}$ is the wind speed. The wind speed is calculated as

$$\bar{w} = \sqrt{u^2 + v^2 + \hat{w}^2}, \qquad (2)$$

where $u$ and $v$ are the monthly averaged zonal and meridional components of the wind, and $\hat{w}$ is a background wind speed used to account for submonthly wind variance (see, e.g., Czaja et al. 2002; we set $\hat{w}$ equal to 4 m s$^{-1}$). Wind speed $\bar{w}$ is defined using the >850-mb vertically averaged wind components. In reality, the bulk formula would use wind speed at a reference height (say, 10 m), so we scale the >850-mb vertically averaged wind speed by 0.8 to account for the reduction of wind speed near the surface. Monthly averaged model data from the CAM3 + SOM control run and the NPO-WARM and NPO-COLD boundary-forced experiments are available for calculating the bulk latent heat flux. The use of monthly mean data in the nonlinear equations for wind speed and saturated specific humidity implies that results are approximate.

The model response in the NPO-forced simulations includes (i) changes in the surface winds that affect the latent heat flux through enhanced vertical transport and (ii) changes to the sea surface temperature that are expected to affect the latent heat flux through changing the vertical humidity gradient. To isolate (i) the effect of zonal wind on the latent heat flux (contours in Figs. 4g,h) we use data from the CAM3 + SOM control simulation for all parameters in Eqs. (1) and (2) except the zonal wind ($u$), which is taken from either the NPO-WARM or NPO-COLD boundary-forced simulation. Similarly, (ii) the contribution of the vertical humidity gradient to the latent heat flux (contours in Figs. 4i,j) is identified using data from the CAM3 + SOM control simulation for calculating the wind speed [Eq. (2)], and using data from the NPO-WARM or NPO-COLD boundary-forced experiment to calculate the vertical humidity gradient ($T_s$, $T_{\mathrm{ref}}$, and RH). The contribution from changes in the meridional wind speed is very small. The sum of estimated contributions from changes in the zonal and meridional winds and changes in the vertical humidity gradient are shaded in Figs. 4e,f and show close correspondence with the actual latent heat flux anomalies (contours in Figs. 4e,f) from the simulations.

Figures 4g and 4i show that during boreal spring the downward latent heat flux anomalies in the NWTP region are caused by the wind anomalies (westerly wind anomalies overly downward latent heat flux anomalies) in the NPO-forced simulations. The contribution of zonal wind anomalies to the latent heat flux in the NWTP region is opposed by changes in the vertical humidity gradient. In general, increases in SST tend to increase the vertical humidity gradient and upward latent heat flux, thus countering the downward latent heat flux anomalies generated by the zonal wind. The eastern subtropics are characterized by large SST anomalies but weak wind anomalies. There, changes in the vertical humidity gradient dominate the latent heat flux anomalies (Fig. 4e). The positive contribution of zonal wind anomalies to the latent heat flux illustrate the importance of wind-induced evaporation and the WES feedback on the development of SST anomalies in the NWTP in response to the NPO.

During the summer, the opposing effects of the wind speed and vertical humidity gradient are closer in magnitude (Figs. 4h,j). This results in a less clearly defined structure for the total latent heat flux (Fig. 4f). An interesting feature during boreal summer is seen in the far western tropical Pacific (around 15°N, 120°E) where westerly zonal wind anomalies (light shading) are associated with very weak and even *upward* latent heat flux anomalies. Furthermore, the large tropical westerly wind anomalies near 15°N, 150°E (Figs. 4h and 2c) do little to reduce the mean upward latent heat flux from the surface. These features will be discussed further in section 5.

## 5. Seasonality and the WES feedback

The WES feedback involves three physical relationships: 1) changes in lower-level winds alter surface

evaporation, 2) evaporation generates SST anomalies, and 3) the SST anomalies affect the lower-level winds. In the present model formulation the second physical relationship, the link between evaporation and SST, is necessarily one in which reduced (increased) evaporation will warm (cool) the surface in a consistent manner. This leaves two physical processes that may be influenced by seasonality in the present model: the sensitivity of surface evaporation to changes in the lower-level wind and the sensitivity of lower-level winds to the development of SST anomalies. For the WES feedback to be positive, warm (cold) SST anomalies need to generate a local relaxation (intensification) of the mean wind speed (e.g., Xie 1999).

### *a. The seasonal cycle of latent heat flux sensitivity*

The effect of the mean state on the surface latent heat flux can be diagnosed by linearizing the bulk latent heat flux formula [Eq. (1)]:

$$\delta \mathrm{LH} = \frac{\partial \mathrm{LH}}{\partial u}\delta u + \frac{\partial \mathrm{LH}}{\partial v}\delta v + \frac{\partial \mathrm{LH}}{\partial T_s}\delta T_s + \ldots. \qquad (3)$$

Each of the partial derivatives indicates the sensitivity of the latent heat flux to a unit change in the respective field. We focus on changes in the zonal wind speed and surface temperature, as the latent heat flux is only weakly sensitive to changes in the meridional wind (not shown). The linear assumption in Eq. (3) is clearly an oversimplification, and as such is used for illustrative purposes here.

The sensitivity of the latent heat flux anomalies to changes in the zonal wind speed is

$$\frac{\partial \mathrm{LH}}{\partial u} = L_v C_e \rho_a [q_{\mathrm{sat}}(T_s) - \mathrm{RH} \cdot q_{\mathrm{sat}} T_{\mathrm{ref}}] \frac{u}{\bar{w}} = \mathrm{LH} \cdot \frac{u}{\bar{w}^2}. \qquad (4)$$

Over the tropical oceans this is negative everywhere where there are mean easterlies, implying that a westerly wind anomaly [positive $\delta u$ in Eq. (4)] will act to decrease the mean upward latent heat flux and warm the surface. Larger *mean* easterlies will imply a larger downward (upward) anomalous heat flux for the same *anomalous* westerly (easterly) zonal wind speed. The sensitivity of the latent heat flux to changes in the surface temperature can be inferred by noting that in general over the ocean $T_{\mathrm{ref}} < T_s$, $\partial T_{\mathrm{ref}}/\partial T_s \approx 1$, $\mathrm{RH} < 1$, and changes in relative humidity are small. Then, the exponential dependence of the Clausius–Clayperon equation implies that an increase in $T_s$ will cause a larger change in $q_{\mathrm{sat}}(T_s)$ than $q_{\mathrm{sat}}(T_{\mathrm{ref}})$, and hence an increase in the vertical humidity gradient. Thus, all else being equal, positive (negative) SST anomalies will tend to increase (decrease) evaporation—a negative feedback.

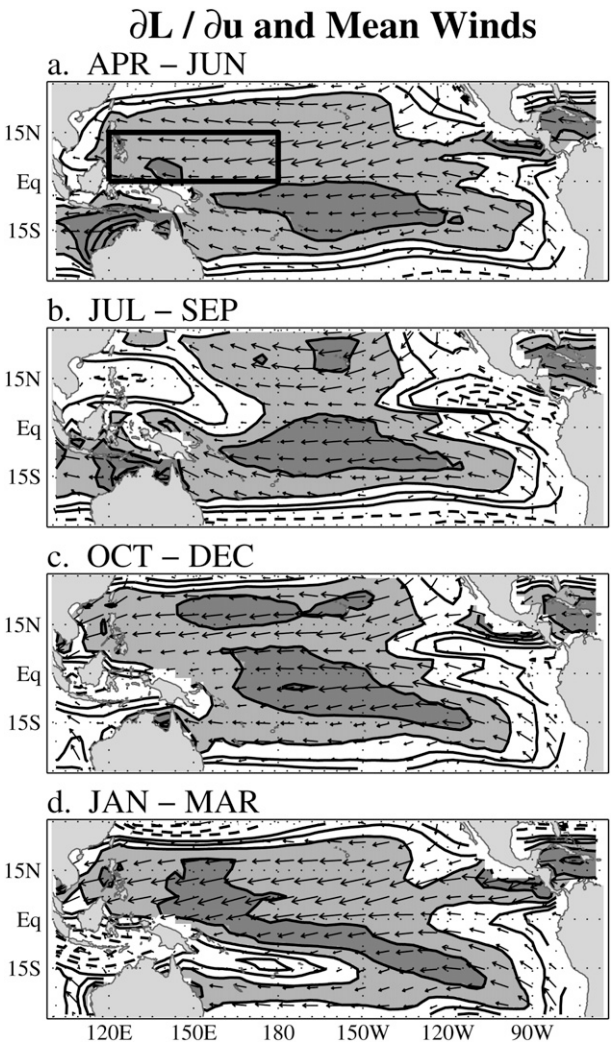


FIG. 5. Latent heat flux sensitivity to changes in the zonal component of the lower-level wind (contours and shading) plotted with the mean wind (vectors) from the CAM3 + SOM control experiment. Data are shown for (a) AMJ, (b) JAS, (c) OND, and (d) JFM. The contour interval for the latent heat flux sensitivity is 5 W s m$^{-3}$, and positive values are shaded. Additionally, medium (dark) shading indicates a sensitivity that exceeds 15 (20) W s m$^{-3}$. Positive sensitivity indicates that a westerly wind anomaly will reduce evaporation, implying a downward anomalous latent heat flux.

The zonal wind sensitivity is plotted with the mean winds from the CAM3 + SOM control experiment in Fig. 5 (polarity is reversed so that positive values indicate a warming of the surface for a westerly wind anomaly). The zonal wind sensitivity demonstrates an important role of the mean state in affecting the strength of latent heat flux feedbacks in the NWTP region. During boreal spring and fall (Figs. 5a,c), the sensitivity is uniformly large (15–20 W s m$^{-3}$) over most

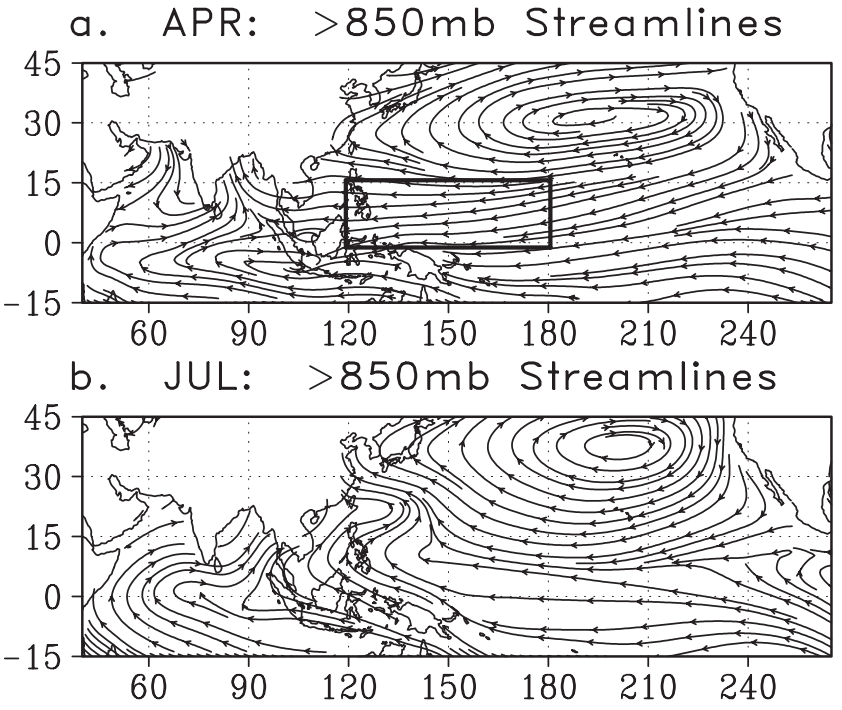


FIG. 6. Streamlines of lower-level winds over the Pacific and Indian Ocean, shown from the CAM3 + SOM control simulation during (a) April and (b) July.

of the tropics consistent with relatively uniform easterly trades over the region. During boreal summer and winter (Figs. 5b,d), two regions of reduced, and even negative, sensitivity emerge in the western summer hemisphere tropics (7.5°–22.5°N, ~120°–135°W in JAS; or west of 180° and between ~7.5° and 15°S during JFM) because of near-zero or westerly mean wind anomalies. This reduction in the zonal wind sensitivity explains the weak negative latent heat flux anomalies in the NWTP region during boreal summer despite the existence of westerly wind anomalies (Figs. 3 and 4h).

The key features of the seasonal cycle that influence this sensitivity, and hence the development of SST anomalies in the NWTP region, may be inferred by examining streamlines of the lower-level wind field over the tropical Pacific and Indian Oceans in Fig. 6. During April, easterly winds extend across the entire Pacific associated with a subtropical high that extends to the western edge of the basin. By July (Fig. 6b) the subtropical high and monsoon trough have migrated to their northernmost positions (around 40°N, 210°E, and 20°N, 150°E, respectively; Hastenrath 1991; Ramage 1995), associated with a region of weak, and even westerly, mean winds between 10° and 25°N and 120° and 150°E. Figure 5b shows that the northward-shifted monsoon trough is related to a reduction, and even reversal in sign, of the latent heat flux sensitivity to zonal wind anomalies. Note that similar features are found in the Southern Hemisphere around 15°S, 165°E, corresponding to the austral summer monsoon (cf. Fig. 5b with Fig. 5d). The sign reversal of the latent heat flux sensitivity demonstrates the importance of the mean seasonal cycle in affecting the evolution of coupled tropical variability associated with the WES feedback. In fact, a similar analysis of observations (using the NCEP–NCAR reanalysis; not shown) indicates that the observed mean westerly monsoon winds are stronger than the modeled mean westerlies; the corresponding observed latent heat flux sensitivity to zonal wind anomalies is larger in amplitude (and more negative—implying that a westerly anomaly will increase evaporation) in nature than in the model.

### *b. Seasonality of the low-level wind response*

In the coupled model experiments, SST anomalies are generated by the imposed heat flux forcing (the directly forced response) and through the coupled response to these directly forced SST anomalies (the coupled WES feedback response). To distinguish the directly forced response from the internally generated response we compare the uncoupled ''CAM3 SST-forced'' and coupled ''IVP'' experiments (Table 1; section 2) in which an idealized SST anomaly is imposed in the eastern

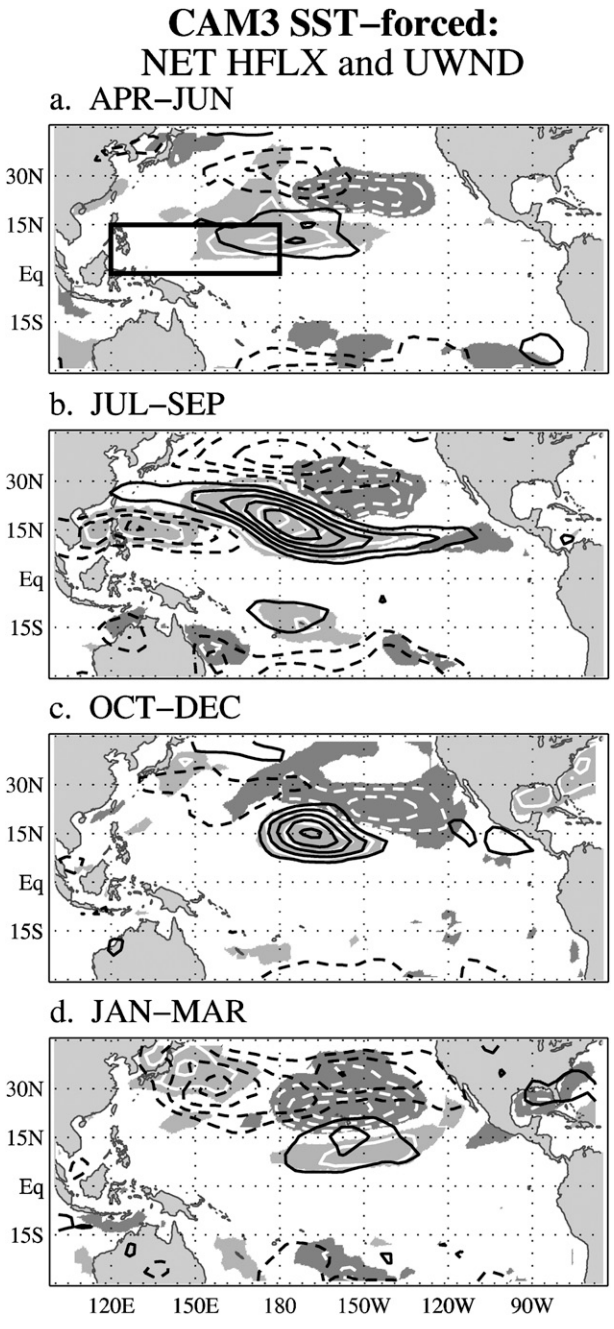


FIG. 7. Lower-level zonal wind (black contours, 0.5 m $s^{-1}$) and net surface heat flux (shaded with white contours, 10 W $m^{-2}$) from the CAM3 SST-forced simulations (SST anomalies are specified as shown in Fig. 8a). Solid lines denote positive values, dashed lines denote negative values, and the zero contour has been omitted.

subtropical Pacific (Fig. 8a). The uncoupled ''CAM3 SST-forced'' experiment illustrates the atmospheric response to (idealized) NPO-generated SST anomalies in the absence of coupled feedbacks. We deliberately focus on forcing from the eastern subtropics to isolate the coupled response in the NWTP region. The IVP simulations impose a heat content anomaly as an initial condition to the CAM3 + SOM model, and as such the atmospheric response includes both the uncoupled response to the idealized NPO SST, as well as the coupled response that evolves through the WES feedback. The coupled response (due to the WES feedback) can be inferred by comparing the uncoupled CAM3 SST-forced experiment (Fig. 7) with the CAM3 + SOM IVP experiments (Fig. 8). In Fig. 8 we show results for boreal summer only, though the main findings are similar during other seasons.

The lower-level zonal wind and net surface heat flux response in the uncoupled CAM3 SST-forced simulation is shown in Fig. 7. These plots demonstrate that the zonal wind response is sensitive to the seasonal cycle. In general, westerly zonal wind anomalies develop to the southwest of the imposed SST anomaly, with the largest amplitude during boreal summer and fall (Figs. 7b,c) and weakest amplitude during boreal spring and winter (Figs. 7a,d). These westerly wind anomalies are collocated with reduced evaporation, which contributes to a downward net surface heat flux. The large zonal wind response in the western Pacific (around 25°N, 120°E–180°) during boreal summer is centered much farther poleward than the response in other seasons. In the far western NWTP region the boreal summer response includes *easterly* lower-level wind anomalies, which, when combined with the weakly negative zonal wind sensitivity in Fig. 5b, actually *reduces* the upward latent heat flux from the surface. This implies that the WES feedback is still positive, despite a negative latent heat flux sensitivity to the zonal wind anomalies in the NWTP region. A comparison of Figs. 5b, 6b, and 7b suggests that the monsoon trough affects both surface evaporation and the structure of atmospheric wind anomalies in the NWTP region.

The uncoupled CAM3 experiments demonstrate that SST anomalies in the subtropical Pacific are capable of directly forcing a wind and heat flux response in the western and central tropical Pacific. Next, we investigate how coupled processes associated with the WES feedback affect these wind anomalies. Wind and SST anomalies are plotted for the months of July–September in the uncoupled CAM3 SST-forced experiment (Fig. 8a), the July IVP experiment (Fig. 8b; corresponding to months 1–3 of the July IVP ensemble experiment), and from the April IVP experiment (Fig. 8d; corresponding to months 4–6 of the April IVP ensemble experiment) in the left column of Fig. 8. For reference, differences between the panels (July IVP

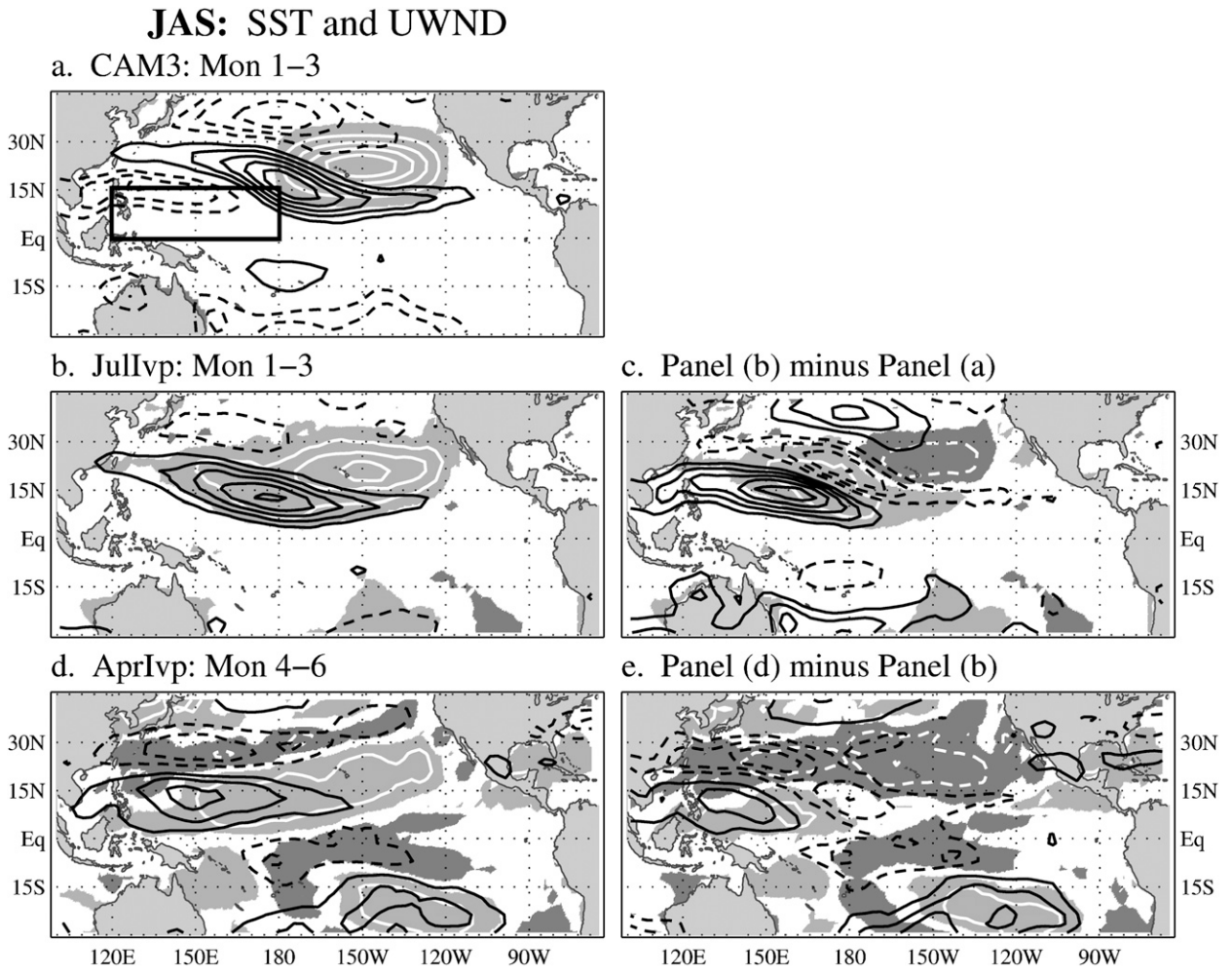


FIG. 8. Lower-level zonal wind (contour 0.5 m $s^{-1}$) and SST (shaded with white contours, 0.2°C) during JAS from (a) the CAM3 SST-forced simulation (SST is specified as shown); (b) months 1–3 of the JulIvp experiment; and (d) months 4–6 of the AprIvp experiment (i.e., all panels show JAS averages). For comparison, (c) the difference between (b) and (a) is plotted, and (e) the difference between (d) and (b) is plotted. Solid lines denote positive values, dashed lines denote negative values, and the zero contour has been omitted.

minus uncoupled CAM3 SST-forced simulation, and April IVP minus July IVP) are plotted in Figs. 8c and 8e, respectively. Note that all panels depict variations during the July–September season.

Figure 8a shows the directly forced (no coupled feedbacks) wind response during boreal summer in the uncoupled CAM3 SST-forced simulation. As discussed earlier, this wind pattern (in its plotted polarity) would tend to generate warm SST anomalies in the NWTP region. This is consistent with the band of warm SST anomalies that develops in Fig. 8b and the difference map in Fig. 8c. Figures 8b,c also show that the zonal wind structure in the CAM3 + SOM July IVP experiment (which includes coupled feedbacks) is shifted southward and slightly westward of its counterpart in the CAM3 SST-forced simulation (which has no coupled feedbacks). The same southwestward shift in the zonal wind response is also prominent in months 4–6 of the April IVP experiment in Fig. 8d (cf. to Figs. 8a,b). Here, the development of warm SST anomalies in the NWTP region during the preceding boreal spring excites westerly wind anomalies that extend down to the equator during boreal summer. In fact, the development of warm SST anomalies in the NWTP region (Fig. 8d) during the preceding boreal spring appears to enhance the southwestward-shifted zonal wind response, even compared to the July IVP simulation (Figs. 8d,e).

The sequence of plots in Fig. 8 demonstrates that coupling plays an important role in the evolution of

variability via the WES feedback in the NWTP region. In particular, coupling with the ocean allows SST anomalies to develop southwest of the imposed SST forcing in the NWTP region. These SST anomalies, in turn, allow lower-level wind anomalies to develop farther equatorward than they would in the absence of coupling. Seasonality appears to play a subtle role in the coupled response as well. The development of warm SST anomalies in the NWTP region during boreal spring in the April IVP simulation (not shown) leads to larger SST anomalies in the NWTP region during the following summer (Fig. 8d), and hence shifts the wind response farther equatorward and westward (Fig. 8e). Similar differences are seen in other months. Although these meridional shifts in the maximum wind anomalies are somewhat subtle, the relatively small oceanic Rossby radius of deformation implies that these shifts may have very different impacts on the equatorial ocean in more physically realistic settings (i.e., in settings where the ocean is able to dynamically respond to the forcing).

## 6. Conclusions and discussion

A series of ensemble model experiments were run to investigate how the tropical ocean–atmosphere system responds to imposed heat flux forcing associated with the midlatitude NPO. The model response demonstrates that the tropical Pacific circulation is sensitive to forcing from the midlatitude atmosphere. The tropical response includes zonal wind anomalies in the central and western tropical Pacific, associated changes in the net surface heat flux (through contributions from the latent and shortwave radiative heat fluxes), and the development of SST anomalies in the northwestern tropical Pacific (NWTP; 15°N–0°, 120°E–180°). Analysis of the latent heat flux indicates that the WES feedback plays an important role in altering the evolution of the response in the NWTP region. In particular, coupling causes zonal wind anomalies to extend equatorward and westward relative to uncoupled simulations. Midlatitude forcing also induces changes in tropical convection, cloudiness, and shortwave radiation. The amplitude of shortwave radiation and latent heat flux anomalies are comparable in the NWTP region, and cooperate in their influence on SST during boreal spring.

In the present model formulation, the mean state and seasonal cycle affect the strength and structure of the WES feedback in two ways: 1) they can alter the sensitivity of latent heat flux anomalies to changes in the surface winds, and 2) they can alter the way that surface winds respond to the SST anomalies. It is shown that the surface latent heat flux is sensitive to the seasonal cycle of lower-level winds, especially in the NWTP region where the seasonal migration of the monsoon trough induces a seasonal reversal of the mean zonal wind. The atmospheric response to SST anomalies (SST anomalies that are directly forced by the NPO or those that develop through the WES feedback) is sensitive to the seasonal cycle as well, with the largest zonal wind anomalies in the western Pacific during boreal summer. Boreal summer, however, is also the time of weakest latent heat flux sensitivity to westerly wind anomalies. So, despite the strong atmospheric response to SST anomalies during boreal summer, the development of SST anomalies in the NWTP region associated with the WES feedback appears to be most effective during boreal spring and fall.

Given the sensitivity of the WES feedback to the background circulation the tropical response to midlatitude forcing will depend on details of the model's (or observed) mean state and seasonal cycle. While the climatology of CAM3 is not perfect, we still expect that many of the results are generally applicable, in particular the southwestward development of SST anomalies through the WES feedback (e.g., Liu 1996) and the reduced heat flux sensitivity to zonal wind variations during the monsoon season (owing to the position of the monsoon trough).

Results from the present study indicate that the WES feedback plays an important role in altering the spatial structure of tropical variability in the western tropical Pacific. In particular, the WES feedback induces a southwestward shift of zonal wind anomalies in the NWTP region, which, though subtle, may play an important role in exciting dynamical changes in the equatorial ocean. Presumably, a dynamical response in the equatorial Pacific Ocean would generate larger equatorial anomalies via physical processes that are absent in the present ocean representation (e.g., upwelling, zonal advection). Future research will include investigation of the NPO's effect on the development of ENSO in more complete physical model configurations (i.e., ocean dynamics).

*Acknowledgments.* This paper is funded by the National Oceanographic and Atmosphere Administration under Grant NA040AR4310139, by NSF under proposal number ATM-0735030, and by the Graduate School at the University of Wisconsin—Madison. NCEP reanalysis data provided by the NOAA/OAR/ESRL PSD, Boulder, Colorado, from their Web site at http://www.cdc.noaa.gov. Thanks to Adam Phillips for providing data for the CAM3 Control simulation.

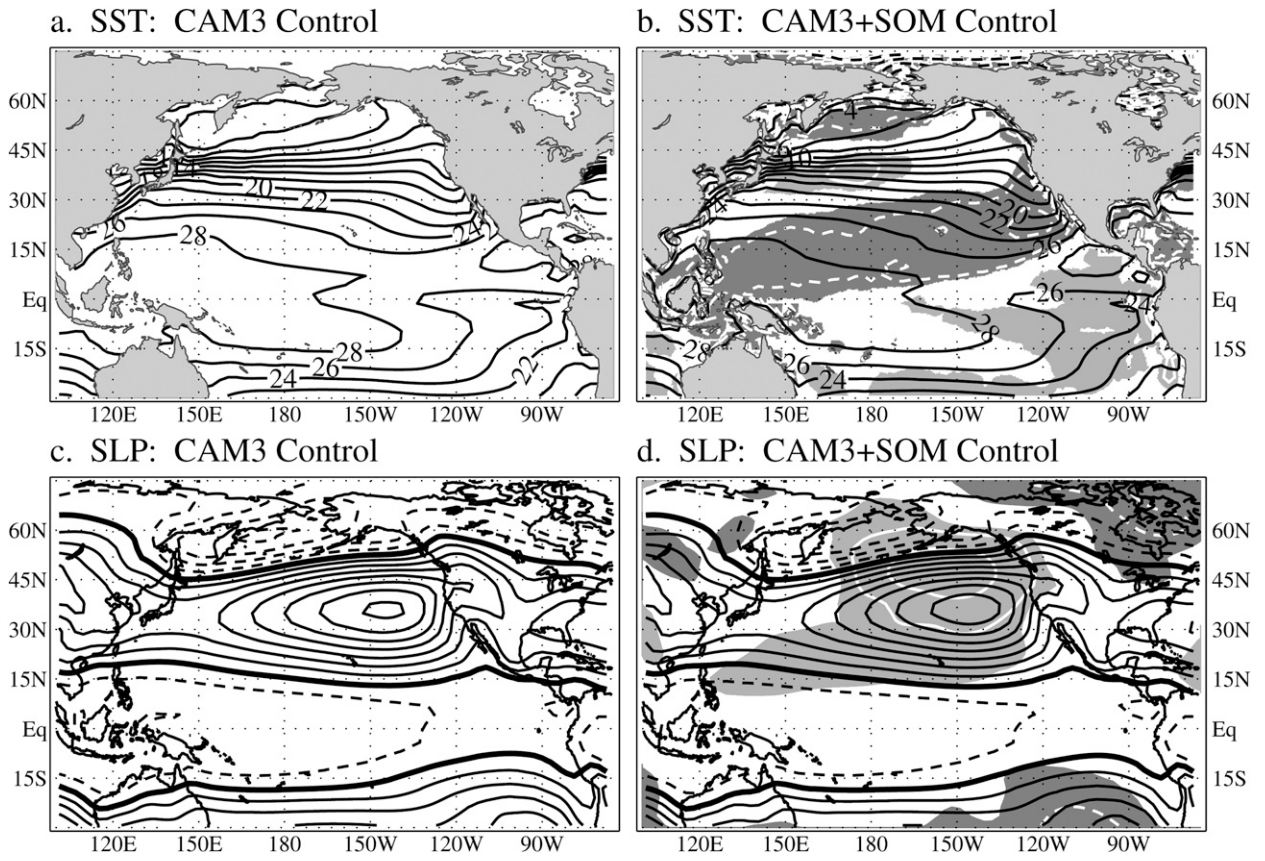


FIG. A1. Mean (top) SST and (bottom) SLP from the (left) CAM3 Control and (right) CAM3 + SOM Control simulations. (a) Annual mean SST (Reynolds et al. 2002) used as a boundary condition for the CAM3 Control simulation, (contour 2°C); (b) annual mean simulated SST from the CAM3 + SOM Control simulation (black contours, 2°C) shown together with the difference between the CAM3 + SOM and CAM3 SST (shading with white contours every 0.25°C); (c) SLP simulated by the CAM3 Control simulation (black contours every 2 mb); (d) SLP simulated by the CAM3 + SOM Control simulation (black contours every 2 mb) shown together with the difference between the CAM3 + SOM Control and CAM3 Control simulation (shading with white contours every 0.5 mb). For SLP, the thick solid contour is the 1013 isobar, solid contours denote pressures greater than 1013 mb (2-mb increments), and dashed contours denote values less than 1013 mb (2-mb increments). For SST and SLP differences [(b) and (d)], solid white contours and light shading denote positive values, dashed contours and dark shading denote negative values, and the zero contour has been omitted.

## APPENDIX A

### CAM3 + SOM Climatology and Q-Flux Calculation

The Q flux for the CAM3 + SOM simulation is calculated as a residual in the surface heat budget for the SOM and represents unresolved ocean heat transport and an attempt to correct for model bias. In general, the vertically integrated heat budget for a constant-depth oceanic mixed layer can be written

$$(\rho c_o H)\frac{d\,\mathrm{SST}}{dt} = F^{\mathrm{net}}_{\mathrm{sfc}} - \nabla\cdot\mathbf{F}_{\mathrm{ocn}}, \qquad \text{(A1)}$$

where the left-hand side represents the storage of heat in a column of water, the first term on the right-hand side represents the net surface heat flux, and the second term on the right-hand side represents the oceanic heat flux convergence. The Q flux is thus calculated as a residual between the storage term (which varies seasonally) and the net surface heat flux:

$$Q = \left[\rho c_o H\frac{d\,\mathrm{SST}}{dt} - F^{\mathrm{net}}_{\mathrm{sfc}}\right]\Big|_{\text{CAM3 Uncoupled}}. \qquad \text{(A2)}$$

An estimate of the net surface heat flux (for the given seasonal cycle of SST) is obtained from the climatology of a long, uncoupled CAM3 simulation that is forced at the surface by the observed seasonal cycle of SST. As such, the Q flux also implicitly includes a correction for the model's net surface heat flux bias.

The mean SST and SLP from years 10–59 of the CAM3 Control simulation and from the CAM3 + SOM simulation are shown in Fig. A1. Figure A1 shows good

agreement between the CAM3 Control (left) and CAM3 + SOM Control (right) simulations, though the CAM3 + SOM Control simulation produces a subtropical high that is stronger and shifted slightly northward (see light shading in Fig. A1b), subtropical SST that is about 0.25°C colder (dark shading in Fig. A1d), and equatorial Pacific SST that is slightly warmer (light shading in Fig. A1d) than counterparts in the CAM3 Control simulation. Both model simulations tend to simulate a subtropical high that is too strong when compared to observations (NCEP reanalysis, 1979–99; not shown).

## REFERENCES


Alexander, M. A., 1992a: Midlatitude atmosphere–ocean interaction during El Niño. Part I: The North Pacific Ocean. *J. Climate,* **5,** 944–958.

——, 1992b: Midlatitude atmosphere–ocean interaction during El Niño. Part II: The Northern Hemisphere atmosphere. *J. Climate,* **5,** 959–972.

——, I. Bladé, M. Newman, J. R. Lanzante, N.-C. Lau, and J. D. Scott, 2002: The atmospheric bridge: The influence of ENSO teleconnections on air–sea interaction over the global oceans. *J. Climate,* **15,** 2205–2231.

——, L. Matrosova, C. Penland, J. D. Scott, and P. Chang, 2008: Forecasting Pacific SSTs: Linear inverse model predictions of the PDO. *J. Climate,* **21,** 382–399.

Ambaum, M. H. P., B. J. Hoskins, and D. B. Stephenson, 2001: Arctic Oscillation or North Atlantic Oscillation? *J. Climate,* **14,** 3495–3507.

Anderson, B. T., 2003: Tropical Pacific sea-surface temperatures and preceding sea level pressure anomalies in the subtropical North Pacific. *J. Geophys. Res.,* **108,** 4732, doi:10.1029/2003JD003805.

——, and E. Maloney, 2006: Interannual tropical Pacific sea surface temperatures and their relation to preceding sea level pressures in the NCAR CCSM2. *J. Climate,* **19,** 998–1012.

Barnett, T. P., D. W. Pierce, M. Latif, D. Dommenget, and R. Saravanan, 1999: Interdecadal interactions between the tropics and midlatitudes in the Pacific basin. *Geophys. Res. Lett.,* **26,** 5615–5618.

Carton, J. A., X. Cao, B. S. Giese, and A. M. da Silva, 1996: Decadal and interannual SST variability in the tropical Atlantic Ocean. *J. Phys. Oceanogr.,* **26,** 1165–1175.

Cayan, D. R., 1992: Latent and sensible heat flux anomalies over the northern oceans: The connection to monthly atmospheric circulation. *J. Climate,* **5,** 354–369.

Chang, P., L. Ji, and H. Li, 1997: A decadal climate variation in the tropical Atlantic Ocean from thermodynamic air-sea interactions. *Nature,* **385,** 516–518.

——, R. Saravanan, L. Ji, and G. C. Hegerl, 2000: The effect of local sea-surface temperatures on atmospheric circulation over the tropical Atlantic sector. *J. Climate,* **13,** 2195–2216.

——, L. Zhang, R. Saravanan, D. J. Vimont, J. C. H. Chiang, L. Ji, H. Seidel, and M. K. Tippett, 2007: Pacific meridional mode and El Niño–Southern Oscillation. *Geophys. Res. Lett.,* **34,** L16608, doi:10.1029/2007GL030302.

Chiang, J. C. H., and D. J. Vimont, 2004: Analogous Pacific and Atlantic meridional modes of tropical atmosphere–ocean variability. *J. Climate,* **17,** 4143–4158.

Collins, W. D., and Coauthors, 2004: Description of the NCAR Community Atmosphere Model (CAM3). National Center for Atmospheric Research Tech. Rep. NCAR/TN-464+STR, 226 pp.

——, and ——, 2006a: The Community Climate System Model version 3 (CCSM3). *J. Climate,* **19,** 2122–2143.

——, and ——, 2006b: The formulation and atmospheric simulation of the Community Atmosphere Model Version 3 (CAM3). *J. Climate,* **19,** 2144–2161.

Czaja, A., 2004: Why is North Tropical Atlantic SST variability stronger in boreal spring? *J. Climate,* **17,** 3017–3025.

——, P. van der Vaart, and J. Marshall, 2002: A diagnostic study of the role of remote forcing in tropical Atlantic variability. *J. Climate,* **15,** 3280–3290.

Hasselmann, K., 1976: Stochastic climate models. I: Theory. *Tellus,* **28,** 473–485.

Hastenrath, S., 1991: *Climate Dynamics of the Tropics*. Kluwer Academic, 488 pp.

——, and L. Heller, 1977: Dynamics of climate hazards in Northeast Brazil. *Quart. J. Roy. Meteor. Soc.,* **103,** 77–92.

Hsu, H.-H., and J. M. Wallace, 1985: Vertical structure of wintertime teleconnection patterns. *J. Atmos. Sci.,* **42,** 1693–1710.

Hu, Z. Z., and B. Huang, 2006: Physical processes associated with the tropical Atlantic SST meridional gradient. *J. Climate,* **19,** 5500–5518.

Kalnay, E., and Coauthors, 1996: The NCEP/NCAR 40-Year Reanalysis Project. *Bull. Amer. Meteor. Soc.,* **77,** 437–471.

Lau, N.-C., 1997: Interactions between global SST anomalies and the midlatitude atmospheric circulation. *Bull. Amer. Meteor. Soc.,* **78,** 21–33.

Linkin, M. E., and S. Nigam, 2008: The North Pacific Oscillation–west Pacific teleconnection pattern: Mature phase structure. *J. Climate,* **21,** 1979–1997.

Liu, Z., 1996: Modeling equatorial annual cycle with a linear coupled model. *J. Climate,* **9,** 2376–2385.

Nitta, T., and S. Yamada, 1989: Recent warming of tropical sea surface temperature and its relationship to the Northern Hemisphere circulation. *J. Meteor. Soc. Japan,* **67,** 375–383.

Okajima, H., S.-P. Xie, and A. Numaguti, 2003: Interhemispheric coherence of tropical climate variability: Effect of climatological ITCZ. *J. Meteor. Soc. Japan,* **81,** 1371–1386.

Pierce, D. W., T. P. Barnett, and M. Latif, 2000: Connections between the Pacific Ocean tropics and midlatitudes on decadal time scales. *J. Climate,* **13,** 1173–1194.

Quadrelli, R., and J. M. Wallace, 2004: A simplified linear framework for interpreting patterns of Northern Hemisphere wintertime climate variability. *J. Climate,* **17,** 3728–3744.

Ramage, C. S., 1995: Forecasters guide to tropical meteorology. Tech. Rep. AWS TR 240, 489 pp.

Reynolds, R., N. Rayner, T. Smith, D. Stokes, and W. Wang, 2002: An improved in situ and satellite SST analysis for climate. *J. Climate,* **15,** 1609–1625.

Rogers, J. C., 1981: The North Pacific Oscillation. *J. Climatol.,* **1,** 39–57.

Trenberth, K. E., G. W. Branstator, D. Karoly, A. Kumar, N.-C. Lau, and C. Ropelewski, 1998: Progress during TOGA in understanding and modelling global teleconnections associated with tropical sea surface temperatures. *J. Geophys. Res.,* **103,** 14 291–14 324.

Vimont, D. J., 2005: The contribution of the interannual ENSO cycle to the spatial structure of decadal ENSO-like variability. *J. Climate,* **18,** 2080–2092.

——, D. S. Battisti, and A. C. Hirst, 2001: Footprinting: A seasonal connection between the tropics and mid-latitudes. *Geophys. Res. Lett.,* **28,** 3923–3926.

——, ——, and ——, 2003a: The seasonal footprinting mechanism in the CSIRO general circulation models. *J. Climate,* **16,** 2653–2667.

——, J. M. Wallace, and D. S. Battisti, 2003b: The seasonal footprinting mechanism in the Pacific: Implications for ENSO. *J. Climate,* **16,** 2668–2675.

Walker, G. T., and E. W. Bliss, 1932: World Weather V. *Mem. Roy. Meteor. Soc.,* **4,** 53–84.

Wallace, J. M., and D. S. Gutzler, 1981: Teleconnections in the geopotential height field during the Northern Hemisphere winter. *Mon. Wea. Rev.,* **109,** 784–812.

Xie, S.-P., 1997: Unstable transition of the tropical climate to an equatorially asymmetric state in a coupled ocean–atmosphere model. *Mon. Wea. Rev.,* **125,** 667–679.

——, 1999: A dynamic ocean–atmosphere model of the tropical Atlantic decadal variability. *J. Climate,* **12,** 64–70.

——, and S. G. H. Philander, 1994: A coupled ocean–atmosphere model of relevance to the ITCZ in the eastern Pacific. *Tellus,* **46A,** 340–350.

——, and Y. Tanimoto, 1998: A pan-Atlantic decadal oscillation. *Geophys. Res. Lett.,* **25,** 2185–2188.

Zhang, Y., J. M. Wallace, and D. S. Battisti, 1997: ENSO-like interdecadal variability: 1900–93. *J. Climate,* **10,** 1004–1020.